ESTIMATION OF VISUAL QUALITY OF INJECTION-MOLDED POLYMER PANELS

J. Jay Liu and John F. MacGregor

McMaster Advanced Control Consortium, Department of Chemical Engineering, McMaster University. Hamilton, ON L8S 4L7 Canada

Abstract

A new machine vision approach for estimating manufactured product appearance is illustrated. This new approach consists of: (1) extraction of textural information from product images, (2) estimation of measures of the visual quality of the product from the textural information extracted. This method is specifically aimed at treating the stochastic nature in the visual appearance of many manufactured products. This non-deterministic nature of product appearance has been a main obstacle for the success of machine vision in the process industries. This approach is successfully applied to an industrial process for estimation of the visual appearance of injection-molded plastic panels.

Keywords: Injection molding, Machine vision, Principal Component Analysis, Visual appearance, Wavelet texture analysis

1 Introduction

The definition of machine vision or computer vision can be given as “interpretation of an image of an object or scene through the use of optical non-contact sensing mechanisms for the purpose of obtaining information and/or controlling machines or processes” [1]. The main purpose of machine vision is “to allow a computer to understand aspects of its environment using information provided by visual sensors” [1] and thus it requires a combination of low-level image processing to enhance the image quality and higher level pattern recognition and image analysis to recognize features present in the image [2]. Machine vision has been studied for about 40 years but the study in last 15 years has shown rapid progress due to the great advances in imaging and computing technologies. The subject of machine vision now embraces innumerable topics and applications: automatic assembly and inspection, automatic vehicle guidance, automatic document interpretation, verification of signatures, checking of fingerprints and recognizing faces, and analysis of remotely sensed images, to list just a few [1,3].

Automatic inspection and assembly is one of the areas where machine vision has been most successfully applied and it is still showing substantial growth. The necessity of improvements in quality, safety, and cost saving is the driving force for this growth. “However, most successful techniques and their applications in this area have been confined to a specific type of environment where certain assumptions can be made about the scene” [1]. In typical manufacturing industries such as microelectronics fabrication, for example, an image provides a scene of objects with pre-determined shape, structure, orientation, and so on, unless the position of a camera changes. In other words, images from such industries are essentially *deterministic*. The primary goal of the inspection in such manufacturing industries is to check whether there are missing objects in pre-specified regions in the image or whether objects in the image are in desired orientations or of desired size, and the necessary analysis is mainly done directly on the image itself; i.e., in image space.

On the other hand, in the process industries there is another class of problems where the major concern is some ill-defined visual appearance of products or processes such as the aesthetics of manufactured countertops, the health of mineral flotation froth [4], or visible patterns on injection-molded polymer panels. In this case, simple assumptions about the scene cannot be made any longer due to the dominantly *stochastic* nature of the visual scene. Therefore, machine vision has seldom been applied to those processes and has had little success when it has. In wood inspection for example, sample-to-sample variation in the grains is too large because natural materials have almost arbitrary shape and orientation. Therefore the state or the quality of these processes or products is almost always judged by trained human operators and any control decisions are left to their discretion at the present time. *Inconsistency* in human judgment still remains a critical issue in the process industries for this reason.

The contribution of this paper is to propose a new machine vision approach for the assessment of the visual quality of manufactured products. In this approach, machine vision will include new application areas and new tasks that have seldom been tried in contemporary machine vision research. New application areas include all process industries where stochastic visual appearance of products or processes is the major concern. New tasks include estimation, modeling, and optimization of visual quality of the process or the product. Visual quality studied in this paper means textural appearance of processes and products. However, it can also include spectral (i.e., color) appearance of products. The rest of this paper is organized as follows: In Section 2, we propose a new machine vision approach by presenting the related theories such as wavelet texture analysis, estimation of visual quality from textural information, and causal modeling of visual quality. This new approach is then illustrated via an application to the visual appearance of injection-molded plastic panels in Section 3. Summary and conclusion are given in Section 4.

2 A New Machine Vision Approach

2.1 Extracting Textural Information Using The Two-Dimensional Wavelet Transform

The appearance or aesthetics of a product usually depend on a combination of color and textural properties of its surface. In the injection-molding application in Section 3 of this paper, the images are grayscale images and appearance is related only to textural properties. Therefore, we will focus on the extraction of textural properties via two-dimensional wavelet transforms. However, there are many works on the extraction of spectral information from color images [5,6] and some recent work on combining both spectral and textural analysis [4,7].

2.1.1 Wavelet Transform

In wavelet analysis, a continuous signal $f(x)$ is decomposed in terms of a family of orthonormal bases $\psi_{m,n}(x)$ obtained through translation and dilation of a mother wavelet $\psi(x)$, i.e.,

$$\psi_{m,n}(x) = 2^{-m/2}\psi(2^{-m}x - n) \qquad (1)$$

where m, n are integers. Due to the orthonormal property, the wavelet coefficients then can be defined as the convolution of the signal with these wavelet bases:

$$c_{m,n} = \int_{\Re} f(x)\psi_{m,n}(x)dx = \left\langle \psi_{m,n}(x), f(x) \right\rangle . \quad (2)$$

The mother wavelet $\psi(x)$ is related to the scaling function $\phi(x)$ with some suitable sequence $h[k]$ [8-10];

$$\psi(x) = \sqrt{2}\sum_k h_1[k]\phi(2x-k) , \quad (3)$$

where $\phi(x) = \sqrt{2}\sum_k h_0[k]\phi(2x-k)$ and $h_1[k] = (-1)^k h_0[1-k]$. Using the following relations, the discrete wavelet transform (DWT) at decomposition level j can be performed without requiring the explicit forms of $\psi(x)$ and $\phi(x)$;

$$\phi_{j,l}[k] = 2^{j/2} h_0[k - 2^j l] , \quad (4)$$

$$\psi_{j,l}[k] = 2^{j/2} h_1[k - 2^j l] . \quad (5)$$

The DWT coefficients of a signal $f(x)$ are now computed as

$$a_{(j)}[l] = \left\langle f[k], \phi_{j,l}[k] \right\rangle \text{ and } d_{(j)}[l] = \left\langle f[k], \psi_{j,l}[k] \right\rangle , \quad (6)$$

where the $a_{(j)}[l]$'s are expansion coefficients of the scaling function or approximation coefficients and the $d_{(j)}[l]$'s are the wavelet coefficients or detail coefficients. In achieving a two-dimensional (2-D) discrete wavelet transform (DWT), there are two different solutions depending on the type of filters and the type of down-sampling lattices [10]. A separable solution (Figure 1a) gives rectangular divisions of frequency spectrum (Figure 1b) and strongly oriented coefficients (often called *subimages* because the wavelet coefficients for 2-D signals are also 2-D) in the horizontal and vertical directions (see Figure 1a). Visible wave patterns in the plastic panels studied in this paper have distinct (or a combination of) orientations and thus a 2-D DWT implemented by the separable solution is suitable for extracting the visible patterns (see images in Section 3).

2.1.2 Wavelet Texture Analysis

Among other texture analysis methods, a 2-D DWT-based method, which is often called *wavelet texture analysis* (WTA) seems best not only because it has shown better performance than other methods in many cases [11,12] but also there is strong psychophysical evidence that the human visual system does multi-channel, space-frequency analysis [13]. WTA has been successfully applied to characterization of steel surface and flotation froth monitoring in previous studies [4,11].

A basic assumption for WTA is that a texture has its unique distribution (i.e., energy or entropy distribution) in the 3-D scale space consisting of the two spatial axes and an additional scale axis. Therefore, if the scale axis of the scale space of a textured image is discretized appropriately, different textures will have different features at the discretized scales. When a wavelet subimage (i.e., $a_{(J)}$ and $d^k_{(j)}$, $j \in \{1, 2, \ldots, J\}$ and $k \in \{h, v, d\}$ for a separable 2-D DWT, Figure 1a) is treated as a matrix, then the power or energy of the subimage can be defined

using the Frobenius norm, $\|\cdot\|_F$. For example, the energy of the detail subimage $d^k_{(j)}$ is given as

$$E_{d^k_{(j)}} = \left\| d^k_{(j)} \right\|_F^2 . \qquad (7)$$

Often this is divided by the number of pixels, yielding averaged power or *normalized energy*. A feature vector composed of energies of all subimages is often called *wavelet energy signature*, one of the most popular wavelet textural features. Other popular features include entropy and averaged l_1-norm of subimages. Since the normalized energy of each subimage is equal to variance of a corresponding channel (after mean-centering for the approximation subimage) the wavelet energy signature also represents contrast information of subimages. Entropy signatures are equivalent to high-order moments of subimages.

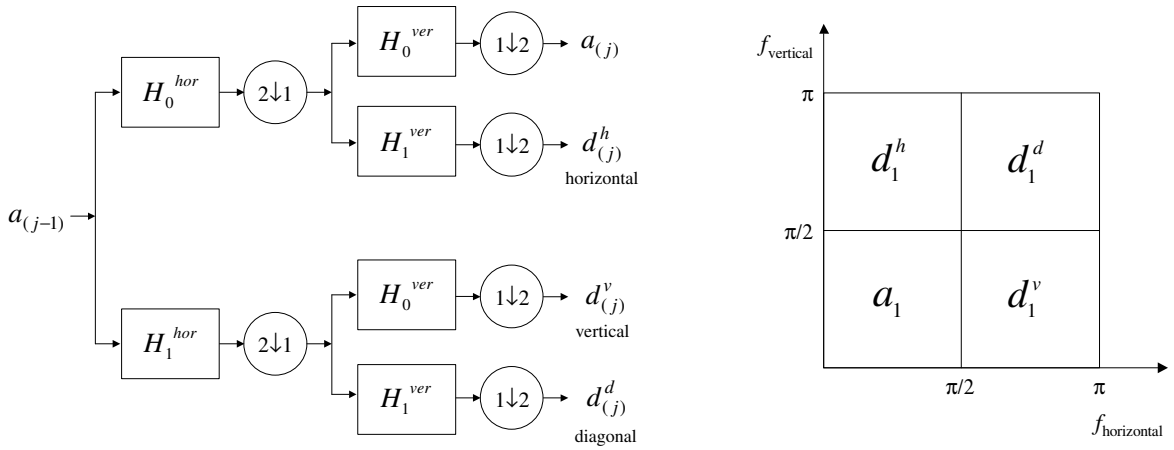

(a) (b)

Figure 1. A separable solution for 2-D DWT. (a) A separable two-dimensional filter bank at the j-th decomposition stage. It consists of horizontal and vertical filtering of 2-D signals using low-pass and high-pass 1-D wavelet filters H0 and H1, and separable horizontal (2↓1) and vertical (1↓2) down-sampling by 2. (b) Division of spatial frequency spectrum by a separable solution for one-level decomposition.

The idea of WTA based on the 2-D DWT can be extended to 2-D wavelet packets (WP) with an arbitrary tree structure [14,15]. When an image is decomposed down to the J-th level, the size of a feature vector for an image (when including an approximation subimage) is $3J+1$ and 4^J for the 2-D DWT and the 2-D full-tree WP, respectively. The approximation subimage is sometimes excluded because the variations induced by lighting or illumination are usually captured in the approximation subimage.

2.2 Estimation of Visual Quality in Latent Variable Spaces

Although a single image can provide an enormous amount of information about the scene depicted, the human visual system can selectively extract the information that is relevant only to specific tasks. Furthermore, the human brain can reduce the dimension of the extracted information and analyze it. For example, operators evaluate the visual quality of steel surfaces as *good*, *medium*, and *bad*, or evaluate the aesthetic quality of manufactured

countertops as *on-specification* and *off-specification* by looking at an image or a scene that can be easily of several megabytes and hundreds of thousands of pixels.

After extracting wavelet textural features (usually much less than 100 features per image) from images, further dimensional reduction can be done using a method such as Principal Component Analysis (PCA) [16-18]. Fisher's Discriminant Analysis (FDA) [19] can be used when class labels are available, and Independent Component Analysis (ICA) [20] and Projection Pursuit (PP) [21] can also be used on the PCA scores (called *pre-whitening* by PCA). All these linear projection methods find an operator (a matrix) that can map high-dimensional feature space to a low-dimensional (usually 2 ~ 4 dimension) latent variable subspace and they are perfect candidates in estimating visual quality. Let $\boldsymbol{f}$ be a $(K\times 1)$ feature vector after 2-D DWT of an image and followed by a nonlinear transform (e.g., $\|\cdot\|_F$) and let $\boldsymbol{t}$ be a $(A\times 1)$ latent vector after dimensionality reduction. Then the following equality holds via a $(A\times K)$ mapping matrix $\boldsymbol{W}$;

$$\boldsymbol{t} = \boldsymbol{W}\boldsymbol{f} \tag{8}$$

The matrix $\boldsymbol{W}$ is called a *loading* matrix in PCA and a *separating* or *unmixing* matrix in ICA.

In any linear projection method, the rows of the mapping matrix represent *contributions* of features $\boldsymbol{f}$ to each of the latent variables in $\boldsymbol{t}$ because each latent variable is simply a linear combination of features with elements in each row of the mapping matrix as coefficients. Therefore if features have certain psychophysical meanings then we can also give a psychophysical meaning to each latent variable. This is crucial when we numerically estimate visual quality and this is the one reason why we choose projection methods. Another reason is that the visual quality of products and/or processes of interest is not a discrete or disjoint quality as in typical classification tasks, rather it is a *continuous* quality [4, 11]; For example, the quality of a steel surface may gradually deteriorate from good to medium and from medium to bad, and the state of a mineral flotation process may gradually change depending upon the amount of chemical reagents added, the mineral content of the ore, and the state of previous flotation cells. Therefore using projection methods and working with continuous latent variables are more suitable in this circumstance than using classification methods and working with discrete class labels.

3 Application to Injection-molded Plastic Panels

3.1 Description of Data

The image data set used consists of 50 grayscale images of injection-molded polymer panels. This data set was obtained via a designed experiment with three operating variables. The variables are polymer formulation, injection speed, and plaque position and the number of levels were five, two, and five respectively. Four samples of the images are shown in Figure 2. Depending on operation conditions, plastic panels can contain visible patterns such as stripes, swirls, and ripples with *varying* characteristics in their shapes, directions, and intensities as shown in the figure. Plastic panels with the desired visual quality have no such visible patterns, i.e., they are visually flat as I074 in the figure. The ultimate goal of this study is to find operating conditions that can produce plastic panels with the visual quality specified by users. The spatial frequency components of the four images in Figure 2 are very different from each

other. I074 has almost zero frequency (DC) components while I243 has very high frequency components (i.e., fine gray dots). I183 and I283 have distinct visible patterns with very low frequency components (e.g., stripes and ripples) as well as some visible patterns with high frequency components.

The main difficulty arises from the fact that there is no distinct class of patterns since different visible patterns can merge together to form more complicated patterns. For example, the four ripples in I183 in Figure 2 are not identical to each other; from top to bottom, the ripple becomes w-shaped (the 2nd the and 3rd ripples) and loses its distinct shape at the bottom. Five arcs in I283 in Figure 2 also show varying characteristics of patterns. There can be an *infinite* number of patterns depending on the number and the types of basic patterns, their varying characteristics, and how they are merged. In general, there is a wide range of stochastic pattern differences in the images.

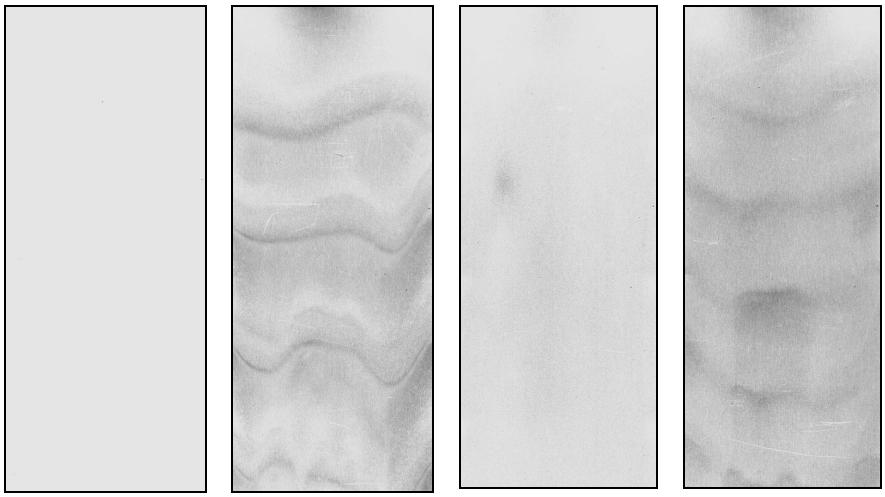

Figure 2. Four samples of pre-processed original images before converted to a grayscale complement. A plastic panel with desired visual quality (I074). Three images with unwanted visual quality (I83, I243, and I283).

3.2 Estimation of Visual Quality

An 1100×2700 image was cropped from each of the original 50 images, down-sampled by 3 to produce 367×900, and finally converted to obtain the complement of the grayscale image. After these pre-processing steps, a 4-level 2-D DWT was applied to each image using order-2 Daubechies filters. These choices were made by trial and error but one can follow some guidelines [15, 23]. Level-one detail subimages of all 50 images showed nothing but irrelevant noise and thus they were excluded from the extracted wavelet feature vectors. All other detail subimages capture horizontal, vertical and diagonal features of the original images. Level 3 and 4 wavelet subimages of I128 are shown in Figure 3 (Figure 3 will help understanding the PCA score space later). The square root of the normalized energy was calculated for each subimage and used as textural features. Therefore each image is represented by a (10×1) feature vector (energies corresponding to a_4 and d_i^h, d_i^v, d_i^d (i = 2, 3, 4)).

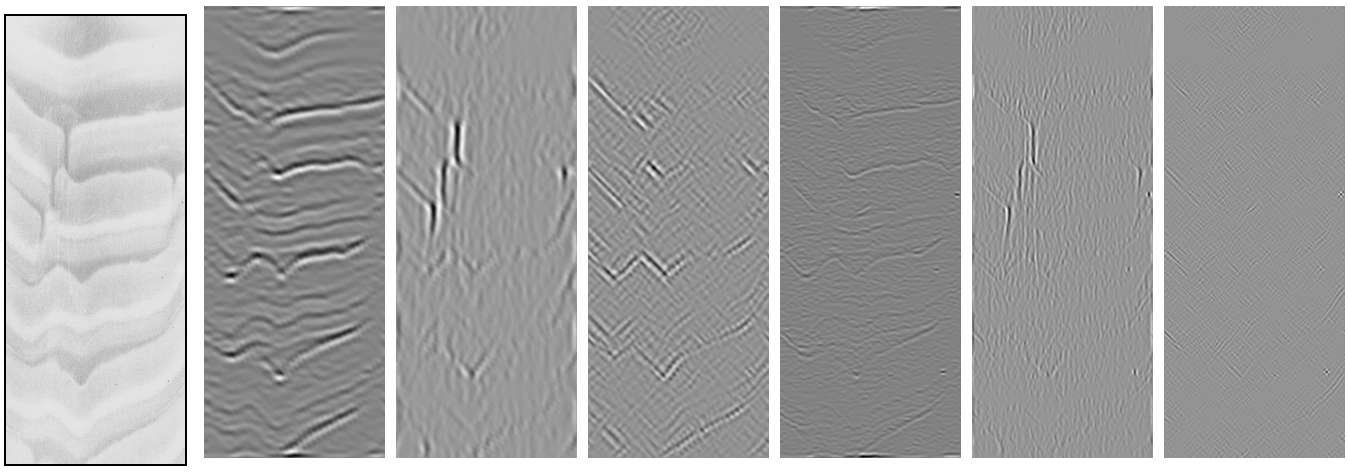

Figure 3. (a) image I128 and (b) some of its wavelet subimages.

Table 1. Summary of Principal Component Analysis results

Dimension of Latent Space	R^2	Q^2
1	0.928	0.916
2	0.971	0.943
3	0.987	0.958
4	0.995	0.970

After auto-scaling, PCA was applied to the (50×10) X matrix where each row consisted of a feature vector for one image. Four statistically significant principal components were found based on Bootstrap risk estimate [24]. R^2 (the fraction of variance of feature vectors explained by the PCA model) and Q^2 (the fraction of variance predicted for images not used in the PCA model) are summarized in Table 1 and a residual plot (distance to the model, DmodX [25]) is given in Figure 4. Clearly, the variability of images in wavelet feature space is well modeled by this PCA model. In order to see whether the four score values of the feature vectors of the images reveal similarity and/or dissimilarity between the visual qualities of the images, a simple nearest-neighbor clustering based on the Mahalanobis distance [26] of score values is applied to all 50 images to find the nearest neighbors of the images in Figure 2. The two nearest neighbors of each of the four images and the corresponding Mahalanobis distances are shown in Figure 5. To give a reference regarding the similarity/dissimilarity between visual quality and the corresponding Mahalanobis distance, the distances between the four images in Figure 2 are listed in Table 2. It is clear from the Figures 2 and 5, and Table 2 that the nearest neighbor images in Figure 5 and corresponding images in Figure 2 are very close in terms of visual quality and in terms of the Mahalanobis distance. As expected from the Figure 2, I283 is the farthest neighbor of I074 (the Mahalanobis distance is 3.614) and the distances between I074 and I243 and between I183 and I283 are 3.049 and 1.831, respectively. By comparing the magnitude of the Mahalanobis distances in Table 2 with those in Figure 5 and comparing the visual similarity/dissimilarity between images in Figures 2 and 5, the principal components do reveal similarity and/or dissimilarity between the visual qualities of images.

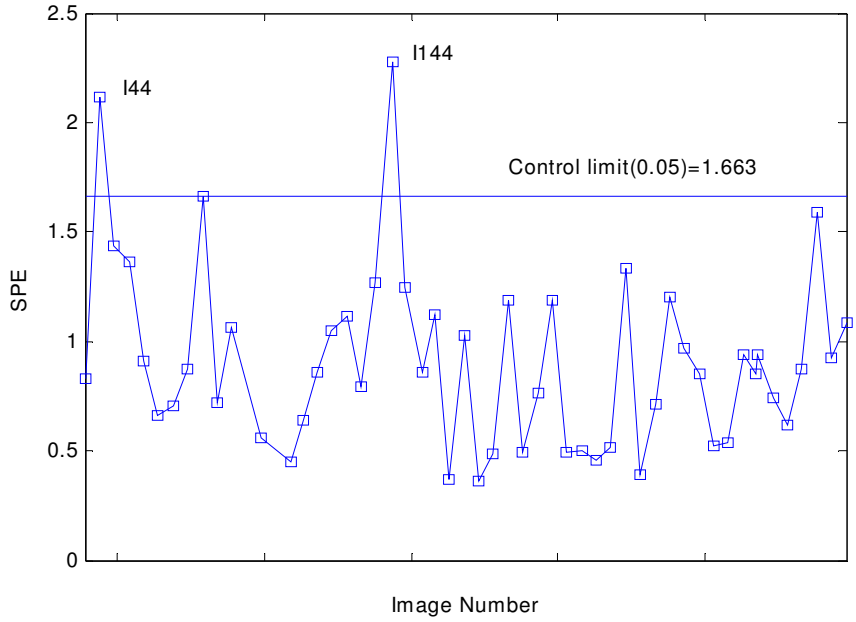

Figure 4. A residual plot for the PCA model

Table 2. Mahalanobis distances between the four images in Figure 2

	I074	I183	I243	I283
I074	0	3.303	3.049	3.614
I183	-	0	3.104	1.831
I243	-	-	0	1.898
I283	-	-	-	0

Loading plots and score plots from the PCA model are shown in Figures 6, 7 and 8. Since the textural signature used in the analysis is equivalent to the standard deviation of wavelet subimages, it represents the *presence of visible patterns* as well as multiresolution *contrast information* of the pre-processed original images. The p_1 loading plot in Figure 6 shows that images in the positive t_1 direction have more contrast in all subimages. In other words, visible patterns in images, whether they are is stripes, swirls, ripples, or fine gray dots, become more and more noticeable when moving toward the positive t_1 direction. To verify this, three images I263, I223, I054 that are at each end and close to the center of the t_1 axis in the t_1-t_2 score plot of Figure 7 are shown in Figure 9. As expected, I263 at the negative end of t_1 axis in the score plot has almost no noticeable visible patterns while I223 at the opposite end of t_1 axis has visible patterns that are strongly noticeable. The visual quality of I054 lies between that of I263 and I223 in *both* the image space and the t_1 score value. On the other hand, the p_2 loading plot in Figure 6 tells that images in the positive t_2 direction have highly-structured visible patterns such as stripes, swirls, and ripples because they have low frequency signals in horizontal, vertical and/or diagonal directions as represented by the big positive p_2 loadings on d_4^h, d_4^v, and d_4^d. Figure 3(b) illustrates how the wavelet subimages capture these low frequency wave patterns. Images in the negative t_2 direction have less structured visible patterns such as fine gray dots. Images I267 (negative t_2) and I133 (positive t_2) in Figure 9

show this behavior. Again the visual quality of I054 is in the middle of I267 and I133 in both image space and the t_2 score value.

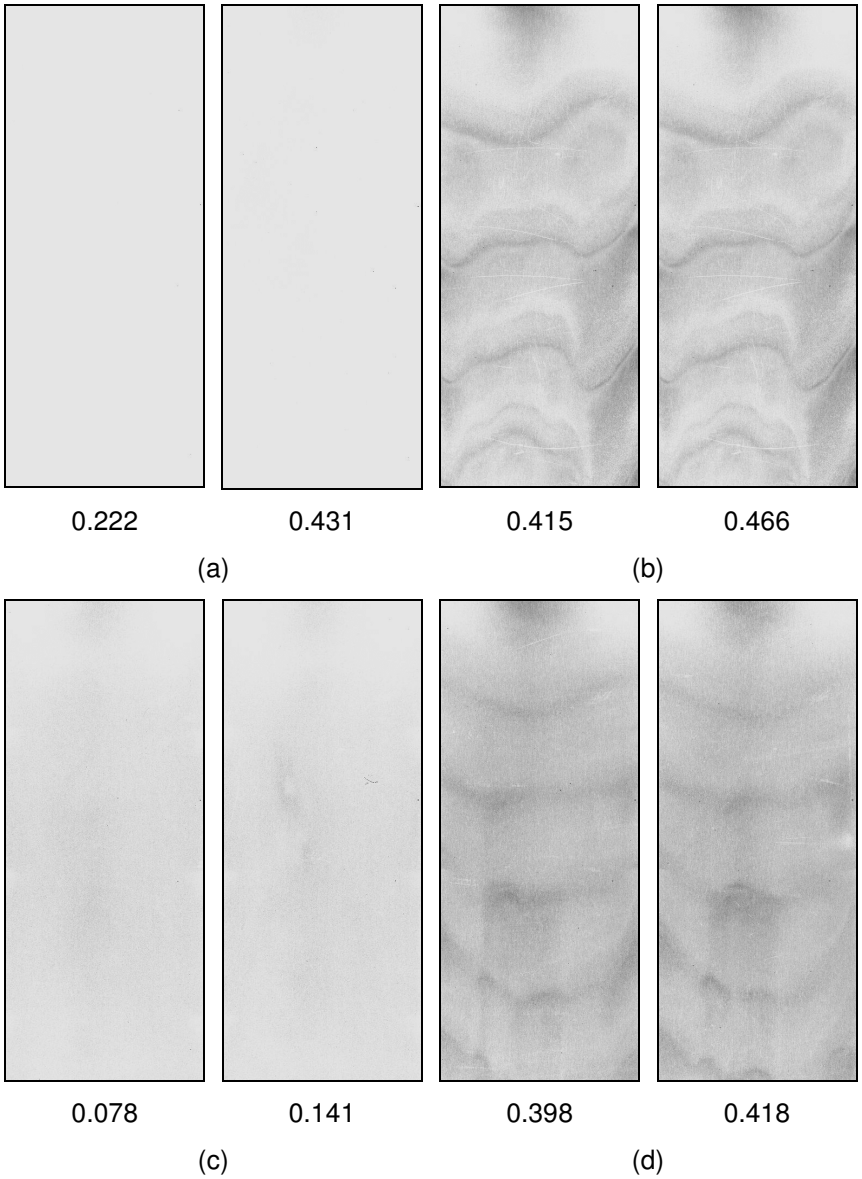

Figure 5 Two nearest neighbors of the four images shown in Figure 2 and corresponding Mahalanobis distances to the images. (a) I263 and I268 for I074 (b) I198 and I188 for I183 (c) I267 and I278 for I243 (d) I293 and I288 for I283

The Psychophysical meaning of the latent variable t_3 can be interpreted in a similar way. It is clear from the p_3 plot that images in the positive t_3 direction will have strongly noticeable vertical patterns (see big positive weights of d_4^v and d_3^v in Figure 6) while images in the negative t_3 direction will have strongly noticeable horizontal patterns (see negative weights of d_4^h and d_3^h in Figure 6). Two images, I123 (negative t_3 in Figure 8) and I228 (positive t_3 in Figure 8), are shown in Figure 10 to verify this behavior. The psychophysical meaning of t_4 is less clear because the score vectors are forced to be orthogonal to previous scores and the most obvious visual characteristics have been explained in t_1~t_3. But from the p_4 plot, images in

the positive t_4 direction should just have darker low frequency background as shown in Figure 6 by high p_4 loading on the approximation a_4. The two images I089 (a negative t_4 score) and I059 (a positive t_4 score) in Figure 10 verify this behavior.

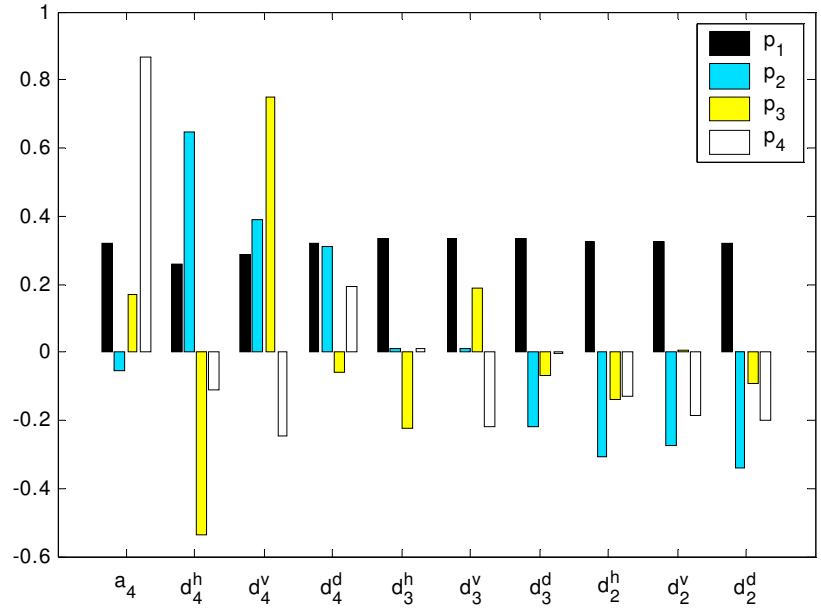

Figure 6 Loading plots for the 4 principal components

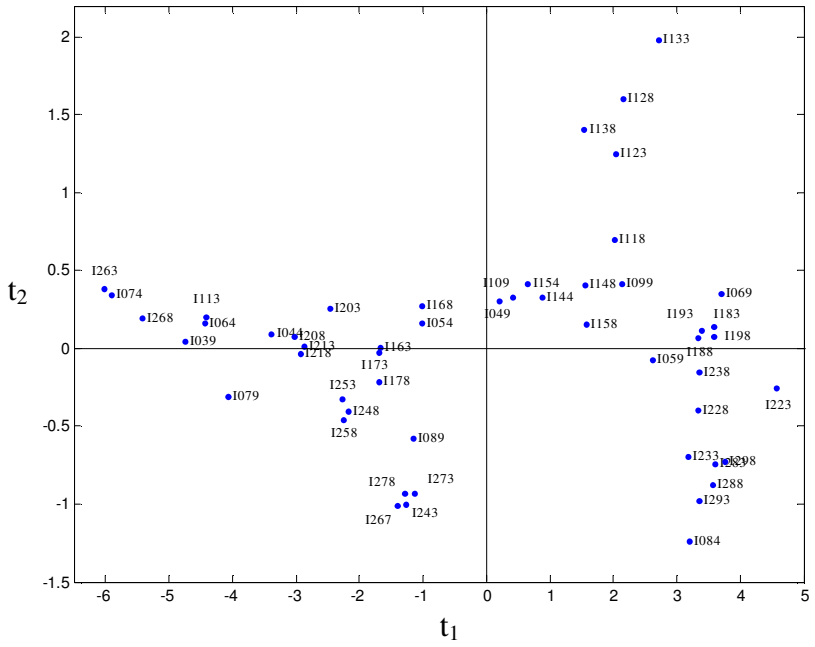

Figure 7 A t_1-t_2 score plot

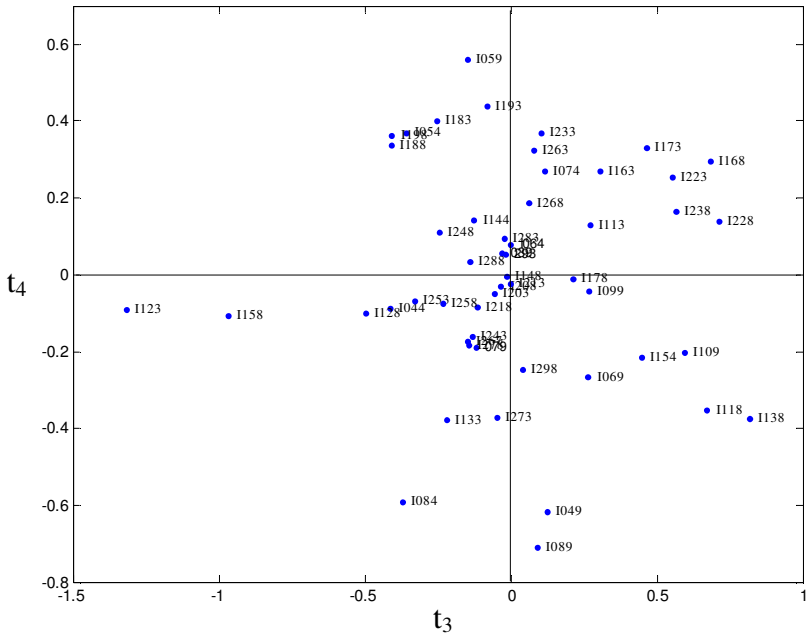

Figure 8 A t_3-t_4 score plot

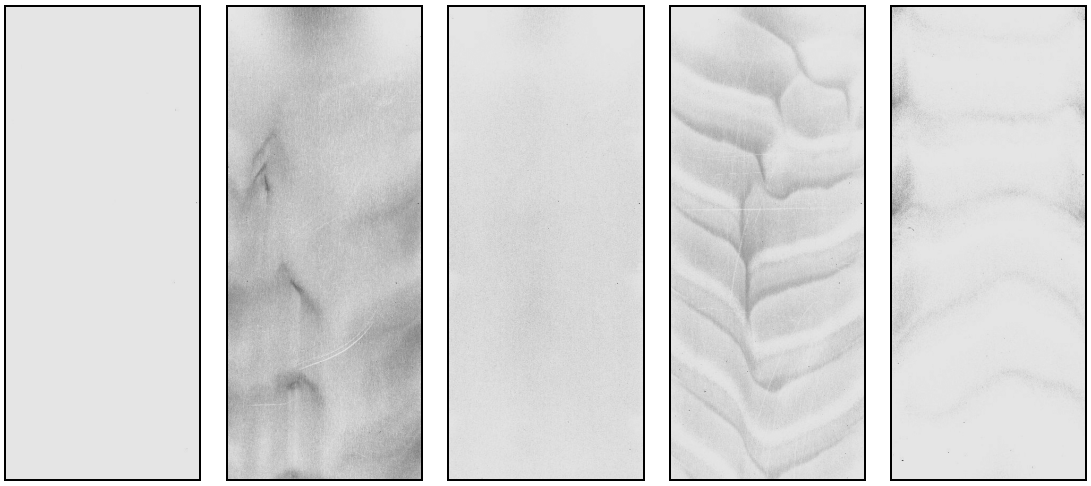

Figure 9 Five selected images in the t_1-t_2 score plot.

4 Conclusion

A new paradigm for machine vision is presented for handling stochastic textural appearance in the process industries. The new machine vision can also be extended easily to include spectral appearance as well by using proper methods [7]. It is applied in this paper for the estimation of the visual quality of injection-molded plastic panels but the new paradigm also opens many opportunities for many systems engineering tasks such as modeling, monitoring, control, and optimization of the visual quality of products or processes. It is also

being applied in a different context to the monitoring and control of the visual appearance of flotation froths in mineral processing [4].

Acknowledgement

Authors would like to thank Dr. Nancy Jestel at GE Advanced Materials for providing the data for this study.

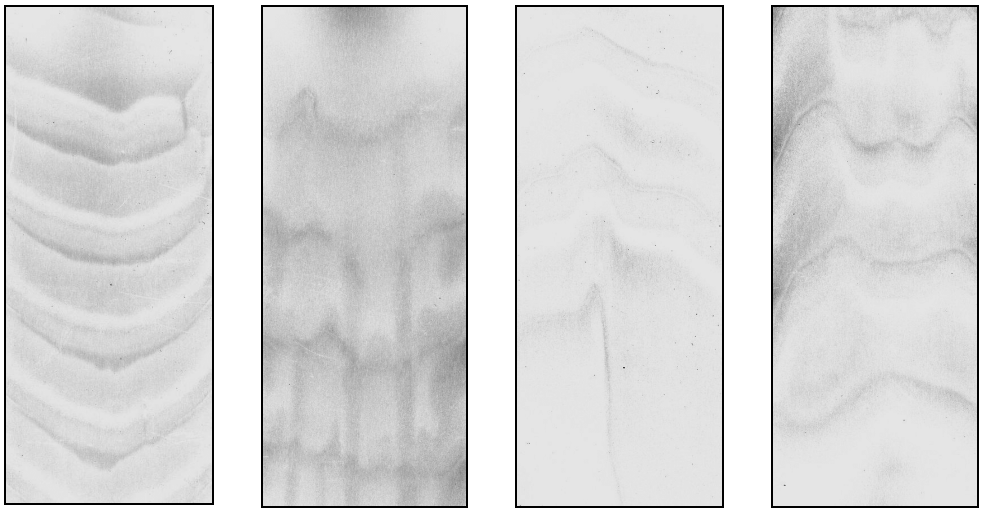

Figure 10 Four selected images in the t_3-t_4 score plot.

Reference

(1) Marshall, A.D; and Martin R.R. *Computer Vision, Models and Inspection*, World Scientific Publishing: Singapore, 1992.
(2) Hyper Dictionary. http://www.hyperdictionary.com/search.aspx?define=computer+vision
(3) Davies, E.R. *Machine Vision: Theory, Algorithms, Practicalities*, 2nd ed., Academic Press: San Diego, 1997.
(4) Liu, J.; MacGregor, J.F.; Duchesne, C., and Bartolacci, G. Monitoring of Flotation Processes using Multiresolutional Multivariate Image Analysis, *Minerals Engineering* **2004**, in press.
(5) Honglu, Y.; MacGregor, J.F.; Haarsma, G.; Bourg, W. Digital Imaging for On-line Monitoring and Control of Industrial Snack Food Processes, *Industrial & Engineering Chemistry Research*, **2003**, 42, 3036.
(6) Honglu, Y.; MacGregor, J.F. Monitoring Flames in an Industrial Boiler Using Multivariate Image Analysis, *AIChE Journal* **2004**, 50, 1474.
(7) Liu, J.; MacGregor, J.F. On the Extraction of Spectral and Spatial Information for Image Analysis, submitted for publication, **2004**.
(8) Mallat, S.G. A theory for multiresolution signal decomposition: The wavelet representation, *IEEE Transactions on Pattern Analysis and Machine Intelligence*, **1989**, 11, 674.
(9) Daubechies, I. *Ten Lectures on Wavelets*, CBMS-NSF Reg. Conf. Series in Applied Math. no. 61, SIAM, Philadelphia, 1992.
(10) Vetterli, M.; Kovačević, J. Wavelets and Subband Coding. Prentice Hall: Englewood Cliffs, NJ, 1995.
(11) Bharati, M; Liu, J.; MacGregor, J.F. Image Texture Analysis: Methods and Comparisons, *Chemometrics and Intelligent Laboratory Systems*, **2004**, 72, 57.
(12) Randen, T.; Husoy, J.H. Filtering for texture classification: a comparative study, IEEE Transactions on Pattern Analysis and Machine Intelligence, **1999**, 21(4), 291.
(13) Tuceryan, M.; Jain, A.K. Texture Analysis, *Handbook of Pattern Recognition and Computer Vision* (ch. 21), 2nd ed., C.H. Chen, et al. eds., World Scientific Publishing Co.: NJ, 1998.
(14) Etdmad, K.; Chellappa, R. Separability-based multiscale basis selection and feature extraction for signal and image classification, *IEEE Transactions on Image Processing*, **1998**, 7, 1453.
(15) Chang, T.; Kuo, C.C.J. Texture Analysis and Classification with Tree-Structured Wavelet Transform, *IEEE Transactions on Image Processing*, **1993**, 2, 429.
(16) Hotelling, H. Analysis of a complex of statistical variables into principal components, *Journal of Educational Psychology*, **1933**, 24, 417.
(17) Karhunen, K. Uber lineare methoden in der Wahrsccheilichkeitsrechnung, *Annales Academiae Scientiarum Fennicae*, Seried A1: Mathematica-Physica, **1947**, 37, 3.
(18) Loéve, M. *Probability Theory*, Van Nostrand: New York, 1963.
(19) Fisher, R.A. The use of multiple measurements in taxonomic problems, *Annals of Eugenics*, **1936**, 7**,** Part II, 179.
(20) Bell, A.J.; Sejnoski, T.J. An information-maximization approach to blind separation and blind deconvolution, *Neural Computation*, **1995**, 7, 1129.
(21) Friedman, J.H.; Tukey, J.W. A projection pursuit algorithm for exploratory data analysis, *IEEE Transactions on Computers*, **1974**, 23, 881.

(22) Moolman, D.W.; Eksteen, J.J.; Aldrich, C.; Van Deventer, J.S.J. The significance of flotation froth appearance for machine vision control, *International Journal of Mineral Processing*, **1996**, 48, 135.
(23) Mojsilović, A.; Popović, M.V.; Rackkov, D.M. On the selection of an optimal wavelet basis for texture characterization, *IEEE Transactions on Image Processing*, **2001**, 19, 2043.
(24) Besse, P.; de Falguerolles, A. Application of resampling methods to the choice of dimension in principal component analysis, *Computer intensive methods in statistics*, W. Härdle and L. Simar, eds., Physica-Verlag: Heidelberg, Germany, pp. 167-174, 1993.
(25) Jackson, J.E. *A User's Guide to Principal Components*, Wiley-Interscience: New York, 1991.
(26) Duda, R.O.; Hart, P.E.; Stork, D.G. *Pattern Classification*, Wiley-Interscience: New York, 2000.